International Journal of Biological Macromolecules 161 (2020) 1371–1380

Contents lists available at ScienceDirect

International Journal of Biological Macromolecules

journal homepage: http://www.elsevier.com/locate/ijbiomac

Stretchable silk fibroin hydrogels

C.B. Oral, B. Yetiskin *, O. Okay *

Department of Chemistry, Istanbul Technical University, Istanbul, Turkey

ARTICLE INFO

Article history:
Received 25 May 2020
Received in revised form 23 July 2020
Accepted 4 August 2020
Available online 10 August 2020

Keywords:
Silk fibroin
Hydrogels
Mechanical properties

ABSTRACT

Hydrogels derived from silk fibroin (SF) are attractive soft materials in biomedical applications such as drug delivery and tissue engineering. However, SF hydrogels reported so far are generally brittle in tension limiting their load-bearing applications. We present here a novel strategy for preparing stretchable SF hydrogels by incorporating flexible polymer chains into the brittle SF network, which strengthen the interconnections between SF globules. We included *N, N*-dimethylacrylamide (DMAA) monomer and ammonium persulfate initiator into an aqueous SF solution containing a diepoxide cross-linker to in situ generate flexible poly (*N,N*-dimethylacrylamide) (PDMAA) chains. Moreover, instead of SF, methacrylated SF was used for the gel preparation to create an interconnected SF/PDMAA network. The free-radical polymerization of DMAA leads to the formation of PDMAA chains interconnecting globular SF molecules via their pendant vinyl groups. Incorporation of 2 w/v% DMAA into the SF network turns the brittle hydrogel into a stretchable one sustaining up to 370% elongation ratio. The mechanical properties of SF hydrogels could be adjusted by the amount of PDMAA incorporated into the SF network. The stretchable and tough SF hydrogels thus developed are suitable as a scaffold in tissue engineering and offer an advantage as a biomaterial over other SF-based biomaterials.

1. Introduction

Silk fibroin (SF) derived from *Bombyx Mori* exhibits unique properties comprising biodegradability, biocompatibility, and ease of processing [1–5]. SF has a block-like biopolymer structure composed of hydrophobic blocks able to induce a conformation transition, and hydrophilic blocks providing its solubility in water [6,7]. The conformation transition of SF in aqueous solutions from random-coil to β-sheet crystals occurs by the associations of hydrophobic blocks via hydrogen bonds leading to the formation of SF hydrogels. Hydrogels derived from SF are attractive soft materials in biomedical applications such as drug delivery and tissue engineering [1,3,8–12]. They have generally been prepared by inducing β-sheet formation in aqueous SF solutions via several triggers such as fibroin concentration [6], solvent quality [13–16], pH [17], temperature [18], cations [19], vortexing [20], electrical field [21] or by chemical cross-linking reactions of native or chemically modified SF [22–27].

However, SF hydrogels reported so far are generally brittle in tension limiting their load-bearing applications. Several attempts have recently been made to prepare flexible SF hydrogels with a high stretchability [15,28–37]. Preparation of interpenetrating network hydrogels based on SF and synthetic or natural polymers provides a slight improvement in their compressive mechanical properties [33,34,38]. Li et al. prepared SF hydrogels sustaining 134% stretch ratio by adding surfactant into aqueous SF solutions and incubating at 60 °C [29]. It was shown that the addition of surfactant strengthens the hydrophobic interactions between SF and surfactant molecules, and hence facilitates formation of β-sheet structures. Incorporation of hyaluronic acid (HA) into a SF hydrogel network enhances its hydrophilicity and improves the tensile mechanical properties [39,40]. HA/SF hydrogels sustain up to 350% stretch ratio under a stress of 70 kPa [39] Double-network (DN) hydrogels composed of interpenetrated SF and hydrophobically modified polyacrylamide networks containing surfactant micelles sustain 0.3 MPa stresses at 800% elongation [30,32]. Low temperature gelation technique (so-called cryogelation) has also been used to improve the mechanical properties of SF hydrogels [41–45]. Yetiskin et al. prepared DN, and triple-network SF cryogels using a diepoxide, 1,4-butanediol diglycidyl ether (BDDE) as a cross-linker in the presence of *N,N,N′N′*-tetramethylethylenediamine (TEMED) as a pH regulator [42]. Although the scaffolds thus produced at SF concentrations above 25 wt% exhibit a high Young's modulus (between 66 and 126 MPa) and compressive strength (between 87 and 240 MPa), they are still brittle in tension similar to the single-network SF cryogels [22]. Thus, previous works reveal that the synthesis of stretchable SF hydrogels is a difficult task and requires a complicated synthetic procedure.

The poor tensile mechanical properties of SF hydrogels can be attributed to the globular structure of SF molecules in aqueous solutions. SF gelation is known to occur via a self-assembly mechanism in which the globular SF molecules are connected each other by β-sheet domains [6,46,47]. Because high segment density inside the globules and inhomogeneous distribution of β-sheet cross-links [28], the

* Corresponding authors.
E-mail addresses: yetiskinb@itu.edu.tr (B. Yetiskin), okayo@itu.edu.tr (O. Okay).

https://doi.org/10.1016/j.ijbiomac.2020.08.040
0141-8130/

interconnections between SF molecules are weak so that SF hydrogels rupture when stretched to a low strain. For instance, Scheme 1a illustrates gelation mechanism of SF using BDDE cross-linker in aqueous solutions. Formation of BDDE cross-links between SF molecules reduces their mobilities because the branched molecules cannot move freely in the solution as compared with free chains (i) [22]. The reduced mobility of SF molecules facilitates the alignment of hydrophobic blocks and hence, formation β-sheet crystals even at a low SF concentration (ii) [22]. However, the resulting 3D fibroin network composed of globular nanoaggregates is brittle, similar to the macroscopic 3D network of microgel particles [48].

We present here a novel strategy for preparing stretchable SF hydrogels by incorporating flexible polymer chains into the brittle SF network to strengthen the interconnections between the SF nanoaggregates. We included *N,N*-dimethylacrylamide (DMAA) monomer and ammonium persulfate (APS) initiator into an aqueous SF solution containing BDDE and TEMED to in situ generate flexible poly(*N,N*-dimethylacrylamide) (PDMAA) which is a biocompatible polymer with associative properties [49–53]. Moreover, instead of SF, methacrylated SF was used for the gel preparation to create an interconnected SF/PDMAA network. As schematically illustrated in Scheme 1b, the free-radical polymerization of DMAA above a certain concentration leads to the formation of PDMAA chains interconnecting globular SF molecules via their pendant vinyl groups (i). The conformation transition in SF at longer reaction times produces hydrogels with a high degree of stretchability (ii). As will be seen below, incorporation of 2 w/v% DMAA into the SF network turns the brittle hydrogel into a stretchable one sustaining up to 370% elongation ratio which is quite high for SF-based hydrogels. What is more, the mechanical properties of SF hydrogels could be adjusted by the amount of incorporated PDMAA that regulates the β-sheet content of SF network. The stretchable and tough SF hydrogels thus developed are suitable as a scaffold in tissue engineering and offer an advantage as a biomaterial over other SF-based biomaterials.

2. Experimental part

2.1. Materials

1,4-butanediol diglycidyl ether (BDDE, Sigma-Aldrich), *N,N,N′,N′*-tetramethylethylenediamine (TEMED, Sigma-Aldrich), *N,N*-dimethylacrylamide (DMAA, Sigma-Aldrich, 99%), glycidyl methacrylate (GM, Sigma-Aldrich, 97%), lithium bromide (LiBr, Merck), ammonium persulfate (APS, Sigma-Aldrich, ≥99%) and sodium carbonate (Na_2CO_3, Merck) were used without further purification. *Bombyx Mori* cocoons were purchased from Koza Birlik (Agriculture Sales Cooperative for Silk Cocoon, Bursa, Turkey).

Separation of silk fibroin (SF) from cocoons and its methacrylation by GM were carried out following a procedure described by Kim et al. [24]: *Bombyx mori* cocoons (~10 g) were cut into small pieces, washed thoroughly with distilled water, and then placed in 1 L of boiling aqueous 0.02 M Na_2CO_3 solution for 1 h to remove sericin proteins. The isolated SF was then rinsed five times in 1 L of distilled water at 70 °C each for 20 min. After drying at 23 ± 2 °C for 2 days, SF (7.0 g) was dissolved in 35 mL aqueous 9.3 M LiBr at 60 °C within 2 h. After addition of GM (2 mL) and stirring for 3 h at 500 rpm, the solution was dialysed in a dialysis tube (10,000 MWCO, Snake Skin, Pierce) for 4 days against distilled water that was changed four times a day. After centrifugation, an aqueous solution of 7 w/v% methacrylated SF (meth-SF) was obtained as determined gravimetrically (Fig. 1a).

2.2. Preparation of hydrogels

The hydrogels were prepared from aqueous solutions of meth-SF and DMAA in the presence of BDDE, TEMED, and APS as the cross-linker, pH-regulator, and initiator, respectively. BDDE concentration was expressed as mmol·g^{-1}, which is mmol of epoxy groups per gram of meth-SF. The concentration of meth-SF in the reaction solution was fixed at 5 w/v%. To find the optimum reaction conditions for the formation of meth-SF hydrogels, the first set of experiments was carried out at various TEMED (0–0.50 v/v%) and BDDE concentrations (0–25 mmol·g^{-1}) in the absence of both DMAA and APS. Typically, to prepare a hydrogel at a BDDE concentration of 20 mmol·g^{-1}, BDDE (1.00 mL) was added to 7.14 mL of aqueous 7 w/v% meth-SF solution under stirring at 23 ± 2 °C. After addition of TEMED between 0 and 0.50 v/v%, the volume of the solution was completed to 10 mL with distilled water. The homogeneous solution was then transferred between the plates of the rheometer instruments as well as into 1 mL plastic syringes of 4.5 mm internal diameter, and the reactions were conducted at 50 °C for 24 h.

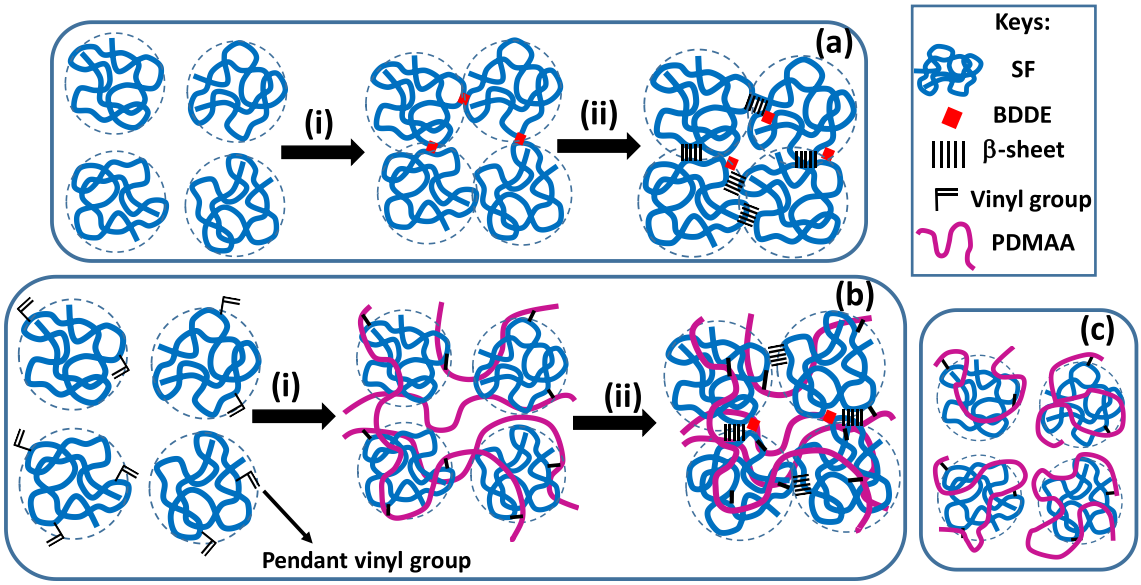

Scheme 1. (a, b): Cartoon showing formation of SF hydrogels via BDDE cross-linker without (a) and with DMAA (b). At low DMAA contents, no gel forms due to the intramolecular reactions (c).

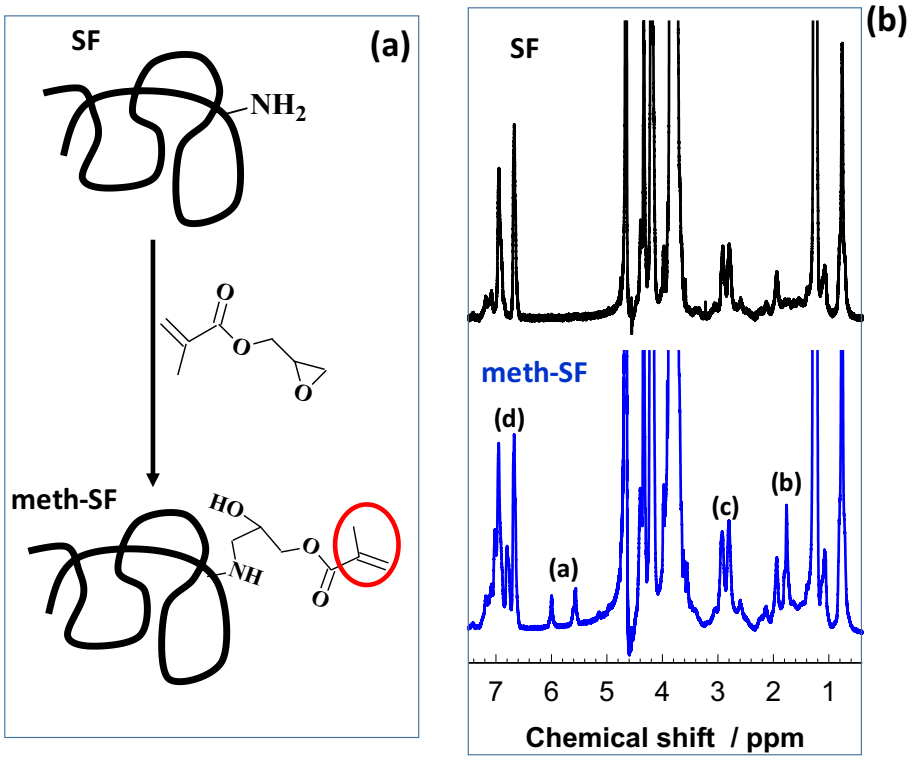

Fig. 1. (a): Methacrylation of silk fibroin (SF) using glycidyl methacrylate (GM) to form methacrylated SF (meth-SF). (b): ^{1}H NMR spectra of SF before (upper panel) and after methacrylation (bottom panel).

meth-SF-DMAA hydrogels were prepared at various DMAA concentrations between 0 and 10 w/v% by fixing TEMED, BDDE, and APS contents at 0.025 v/v%, 20 mmol·g^{-1}, and 3.51 mM, respectively. Both TEMED and APS were used as stock solutions in distilled water of concentrations 0.5 v/v% and 8 w/v%, respectively. Typically, to prepare a hydrogel with 3 w/v% DMAA, a 7.14 mL aqueous solution of 7 w/v% meth-SF was mixed with DMAA (0.31 mL), BDDE (1.00 mL), and the stock solutions of TEMED (0.5 mL) and APS (0.10 mL). After completing the final volume to 10 mL with distilled water, the homogenous solution was transferred between the plates of the rheometer as well as into plastic syringes as described above to conduct the gelation reaction at 50 °C for 24 h.

2.3. Characterization

Methacrylation degree of SF was determined by ^{1}H nuclear magnetic resonance (NMR) spectroscopy on a 500 MHz Agilent VNMRS NMR instrument using SF specimens before and after methacrylation, that were dissolved in D_2O at a concentration of 10 mg·mL^{-1} (Fig. 1b). X-ray diffraction (XRD) and Fourier transform infrared spectroscopy (FTIR) in attenuated total reflectance (ATR) mode were employed to determine the conformation of SF in the hydrogels. XRD patterns of freeze-dried samples were recorded on a PANalytical X-Pert PRO Multi-Purpose Diffractometer using Ni-filtered CuKα (λ = 0.15418 nm) radiation at 45 kV and 40 mA in the range of 2θ = 5–40°. ATR-FTIR spectra of freeze-dried hydrogel samples were recorded on an Agilent Technologies Cary 630 ATR-FTIR spectrophotometer. The conformation of fibroin was estimated by analyzing the spectra using PeakFit software (Version 4.12, SeaSolve Software Inc.). Linear base line correction was applied to the amide I region (1580–1720 cm^{-1}) representing the carbonyl stretching vibration of amide groups. Amide I band was deconvolved into four components each of which was then curve-fitted using a Gaussian model [22,23]. For the curve fitting procedure, the peak positions at 1620, 1640, 1660, and 1698 cm^{-1}, representing β-sheet, random coil, α-helix, and β-turn conformations, respectively, were fixed, and the peak widths and heights were varied freely [54,55]. The areas under the peaks were then determined to estimate conformation percentages (Fig. S1). We have to mention that the assignment of the peaks at around 1650 cm^{-1} is controversial, with some authors attribute these to random coil while others to silk I conformation [56–59].

Rheological measurements were conducted on a Gemini 150 Rheometer system (Bohlin Instruments) equipped with a Peltier device for temperature control, and a solvent trap to minimize the evaporation of water. To monitor the gelation reactions, a cone-and-plate geometry with a cone angle of 4° and diameter of 40 mm was used as the measuring system. The reaction solutions were pipetted between the plate and the cone of the instrument at 50 °C. The storage modulus G', loss modulus G'', and the loss factor tan δ of the reaction solution at a frequency ω of 6.28 rad·s^{-1} and a strain amplitude γ_o of 1% were monitored as a function of the reaction time t. The limiting modulus G'_∞ of meth-SF-DMAA hydrogels at the plateau regime was estimated by fitting G' vs t data to the Hill equation [60–62],

$$G'(t) = G'_\infty \frac{t^n}{t^n + \theta^n} \quad (1)$$

where θ and n are constants (Fig. 4a). Frequency sweep tests at γ_o = 1% were carried out on cylindrical hydrogel discs prepared in 50 mL plastic syringes of 28 mm in diameter, as described above, using a parallel plate geometry (diameter 20 mm) as the measuring system with a gap size of 1000 ± 200 μm depending the specimen thickness.

Uniaxial tensile and compression tests were conducted at 23 ± 2 °C using a Zwick Roell Z0.5 TH model universal test machine equipped with a 500 N load cell. The nominal stress σ_{nom} and the strain ε (change in the sample length / initial sample length) were recorded at a fixed strain rate of 1.7 min^{-1}. The compressive strength was calculated from the maxima of true stress-strain curves, as detailed before [63].

Young's modulus E was determined from slope of σ_{nom} - ε curves between 5 and 15% deformation. Cyclic compressive tests were conducted at the same strain rate by conducting five successive loading-unloading steps to a predetermined maximum strain without a wait time between the cycles.

Swelling tests were conducted by cutting the hydrogels taken out of the syringes into small pieces of about 5 mm in length and then placing them in an excess of distilled water at 23 ± 2 °C for 3 days by replacing water every day. After reaching the swelling equilibrium, the specimens were dried using a freeze-dryer (Christ Alpha 2–4 LD plus) by first freezing at −80 °C, freeze-drying at −40 °C/0.12 mbar and final drying at −60 °C/0.01 mbar, each for one day. The equilibrium weight swelling ratio q_w was calculated as $q_w = m / m_{dry}$, where m and m_{dry} are the swollen and dried masses of the hydrogels, respectively. The soluble fraction of the hydrogels was calculated from masses of dried polymer and meth-SF + DMAA in the reaction solution.

3. Results and discussion

As mentioned in the introduction, SF hydrogels prepared from native SF using BDDE cross-linker exhibit a high Young's modulus but fractures at very low strains during stretching. To generate stretchability, DMAA monomer was included into the SF gelation system together with APS initiator to in situ generate flexible, biocompatible PDMAA chains. Moreover, instead of SF, methacrylated SF (meth-SF) was used for the gel preparation to create an interconnected SF/PDMAA network. meth-SF was prepared by methacrylation of SF using glycidyl methacrylate (GM) in an aqueous LiBr solution (Fig. 1a) [24]. Formation of meth-SF was proved by NMR spectra of SF before and after methacrylation (Fig. 1b). Compared to native SF, meth-SF shows new signals at δ = 6.2–6.0 and 5.8–5.6 ppm due to the methacrylate vinyl groups (a), and at δ = 1.8 ppm due to the methyl group of GM (b) (Fig. 1b). Moreover, the signal of lysine methylene at δ = 2.9 ppm (c) decreased after methacrylation of native SF indicating the reaction of its lysine amino groups with GM. The signal of aromatic amino acid protons at δ = 6.9–7.5 ppm (d) was used to normalize the spectra. The degree of methacrylation (DM) defined as the fraction of lysine residues in SF reacted with GM was calculated as $DM = 1 - I/I_o$ where I_o and I are the integrated signals of lysine methylene before and after the reaction, respectively [24]. In this study, the amount of GM was fixed at 0.3 mL per gram of SF leading to a methacrylation degree of 14%.

In the following first section, we present the properties of meth-SF hydrogels prepared at various TEMED and BDDE concentrations in the absence of DMAA. The second section shows the effect of DMAA incorporation at various concentrations on the hydrogel properties.

3.1. meth-SF hydrogels

Gelation of meth-SF at a concentration of 5 w/v% was conducted at 50 °C in the presence of BDDE and TEMED as a cross-linker and pH regulator, respectively. To optimize the synthesis conditions of meth-SF hydrogels, TEMED amount was first varied between 0.025 and 0.5 v/v % at a fixed BDDE content of 20 mmol·g^{-1}. Fig. 2a shows the storage modulus G' of the reaction solutions with varying TEMED content as a function of the reaction time. The variation of pH of the reaction solution depending on the TEMED content is also shown in Fig. 2b. No gel could be obtained in the absence of TEMED, i.e., at pH = 5.8, while incorporation of 0.025 v/v% TEMED increases pH to 7.4 and leads to the formation of a hydrogel with around 100 kPa modulus. The results also show that both G' and the induction period decrease as the TEMED content, i.e., pH of the reaction system is increased. Thus, the highest modulus, i.e., cross-link density was obtained at pH = 7.4 while it decreases but the reaction occurs faster at higher pH values. This finding is in accord with a previous report on the cross-linking of collagen in aqueous solutions using BDDE cross-linker [64]. At pH = 9, the cross-linking reactions between the amino groups of collagen with BDDE proceeds at a low reaction rate but with a high cross-link efficiency, especially after prolonged reaction times. At a higher pH, although the reactions are faster, the cross-linking efficiency substantially decreases [64].

Fig. 2c shows G', the loss modulus G'', and loss factor $tan\ \delta$ of the reaction system after 4 h of reaction time plotted against pH. G' is 120 kPa at pH = 7.4 while it rapidly decreases above pH = 9 and becomes 30 Pa at pH = 11.2, which is more than 3-orders of magnitude smaller than that measured at pH = 7.4. Moreover, the loss factor is below 0.1 for all hydrogels revealing that they are so-called "strong gels" with a low extent of energy dissipation during the oscillatory deformation tests [65,66]. XRD and FTIR measurements were conducted on dried hydrogels to characterize the conformation of fibroin in the hydrogels. Fig. 3a shows XRD patterns of the hydrogels formed at various pHs together with the neat meth-SF and SF for comparison. Similar to SF, meth-SF shows a broad peak near 21° corresponding to a random coil conformation. After gelation of meth-SF, a distinct peak at 20.1° and a minor peak at around 9° appear corresponding to spacing distances of 0.44 and 0.98 nm, respectively. These spacings are typical for β-sheet crystalline structure of silk fibroin [17,23,67]. The peak at 20.1° becomes broader as the pH increases indicating decreasing β-sheet content of the hydrogels. Fig. 3b shows amide I region of the FTIR spectra for the hydrogels prepared at various pHs together with the neat SF and meth-SF, shown by the open symbols. meth-SF before gelation exhibits a broad peak at 1640 cm^{-1} corresponding to random coil conformation [54,55], while this peak disappears after gelation and three new peaks appear at 1620, 1660, and 1698 cm^{-1} assigned to β-sheet, α-helix, and β-turn conformations, respectively [55]. The conformation percentages of meth-SF in the hydrogels were estimated by analyzing the peak positions at 1620, 1640, 1660, and 1698 cm^{-1} (Fig. S1). The variation of β-sheet content of the hydrogels depending on pH shows a similar trend as the storage modulus G' (Fig. 3c vs Fig. 2c); the higher the pH of reaction system, the lower is both the β-sheet content and the modulus G' indicating that the β-sheet domains serve as cross-link points forming the 3D network structure of meth-SF hydrogels.

The soluble fraction f_{sol} of the hydrogels in water and their equilibrium swelling ratios q_w are other means of studying the cross-link density of the hydrogels. Fig. 3d shows f_{sol} and q_w of the hydrogels plotted against pH of the gelation solution. Both f_{sol} and q_w increase with increasing reaction pH and finally, the hydrogels become completely soluble in water at the highest pH of 11.2. All these findings indicate that meth-SF hydrogels with a modulus of around 100 kPa that are stable in water can be obtained at a pH between 7.2 and 9.2. Another synthesis parameter that may affect the hydrogel properties is the amount of BDDE cross-linker. Experiments were also conducted by fixing pH at 7.4 and varying BDDE content between 0 and 25 mmol·g^{-1}. Rheological measurements showed no gel formation at or below 5 mmol·g^{-1} while between 15 and 25 mmol·g^{-1}, hydrogels with a modulus of around 100 kPa could be obtained (Fig. S2).

All meth-SF hydrogels reported above were brittle to be clamped for the tensile testing. This behavior is similar to the BDDE cross-linked hydrogels derived from native SF due to the weak interconnections between globular SF molecules [22]. In the following section, DMAA was included into the reaction system to create flexible PDMAA chains strengthening the brittle meth-SF network.

3.2. meth-SF-DMAA hydrogels

The optimum reaction conditions for the preparation of meth-SF hydrogels, namely pH = 7.4 and BDDE = 20 mmol·g^{-1} were fixed while DMAA between 0.5 and 10% (w/v%, same meaning throughout the text) together with APS initiator (3.51 mM) were included into the reaction solution. We have to note that because meth-SF concentration was fixed at 5 w/v %, dividing DMAA % by 5 gives the mass-to-mass ratio of DMAA/meth-SF. Fig. 4a shows the variation of the storage modulus G' during the gelation reactions at 50 °C and at various DMAA contents. Interestingly, although a hydrogel with G' of around 100 kPa

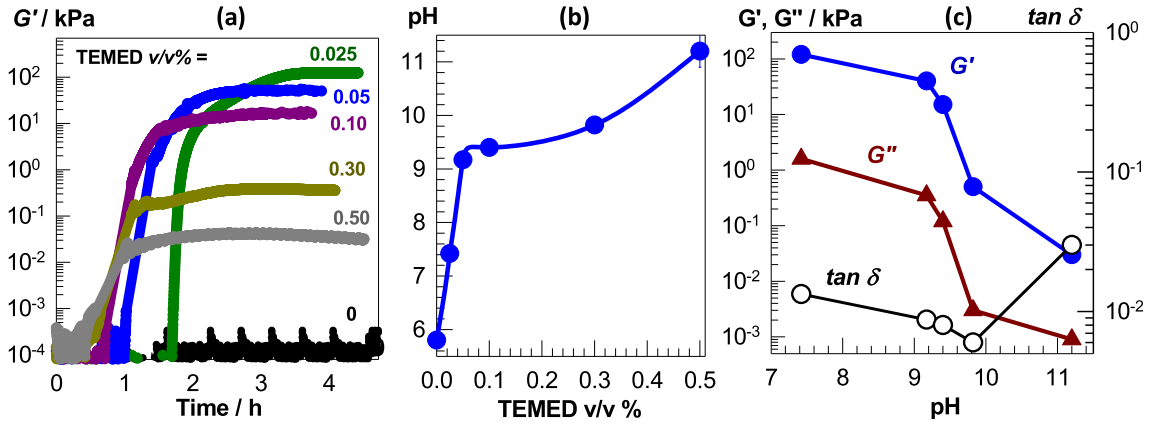

Fig. 2. (a): Reaction time dependence of storage modulus G' of the gelation system at various TEMED contents as indicated. $\omega = 6.28$ rad·s^{-1}. $\gamma = 0.01$. (b): pH of the reaction solution plotted against TEMED %. (c): G', loss modulus G'', and loss factor $tan\ \delta$ after a reaction time of 4 h plotted against pH of the reaction solution.

forms in the absence of DMAA, the presence of 0.5–2% DMAA prevents the increase in the modulus and hence the onset of gelation, while at higher DMAA contents, hydrogels are again formed. This suggests that DMAA at small amounts suppresses the conformation transition in meth-SF which can be supported from the appearance of the hydrogels (Fig. 4b). DMAA-free hydrogel after a reaction time of 24 h is fully opaque whereas the hydrogel with 3% DMAA is almost transparent. With increasing DMAA content from 3 to 10%, the hydrogels become gradually opaque indicating formation of increasing amount of β-sheet domains acting as scattering centers for light. Another characteristic feature of the hydrogels is their two-step formation process (Fig. 4a): After an induction period, G' first rapidly increases and attains a plateau value at around 1 kPa. After passing the plateau, a second rise in G' appears at longer reaction times. However, this second reaction step could not be followed due to the inertia effects in the rheometer leading to a large scatter in the moduli data. The solid curves in Fig. 4a are the best fits of the data in the second reaction step to the Hill equation, as detailed in the experimental part. To check the reproducibility of the limiting G' data obtained from the fits, they were compared with the measured data of the hydrogels after a reaction time of 24 h (Fig. S3). At 3, 5, and 10% DMAA, the limiting G' values predicted are 21, 57, and 117 kPa as compared to the experimental data of 24, 62, and 105 kPa, respectively, indicating a deviation of less than 12%. The results show that the higher the DMAA content, the shorter is the length of the plateau between the two steps, and the higher is the final modulus of the hydrogels. We can explain the two-step reaction profile with the occurrence of two successive cross-linking reactions in the reaction system, as similar to the SF/HA gelation system in the presence of DMAA [39]. In the first step, the polymerization of DMAA in the presence of meth-SF acting as multifunctional cross-linker leads to the formation of meth-SF cross-linked PDMAA hydrogels with a modulus of around 1 kPa. Because the conformation transition in SF needs longer times [22,39], the formation of β-sheet domains during the second gelation step produces additional cross-links in the hydrogels. To proof this mechanism, the gelation reaction in the presence of 3% DMAA was repeated in the absence of BDDE at a reduced temperature, 25 °C, to prevent β-sheet formation. As seen by the gray curve in Fig. 4a, G' increases up to around 1 kPa and then remains almost unchanged at longer times, supporting the above explanation.

To characterize the conformation of fibroin in the hydrogels, FTIR and XRD measurements were conducted on dried hydrogels at various DMAA contents (Fig. 5a, b). Although amide I region of FTIR spectra of the hydrogels exhibits the characteristic peak of β-sheet domains at 1620 cm^{-1}, this peak overlaps with the broad peak at 1626 cm^{-1} of pure PDMAA polymer (dashed line in Fig. 5a), preventing quantitative determination of the β-sheet contents. However, the sharper peak at 1620 cm^{-1} for the hydrogels as compared to that for PDMAA indicates formation of β-sheets during gelation. In XRD scans, the two

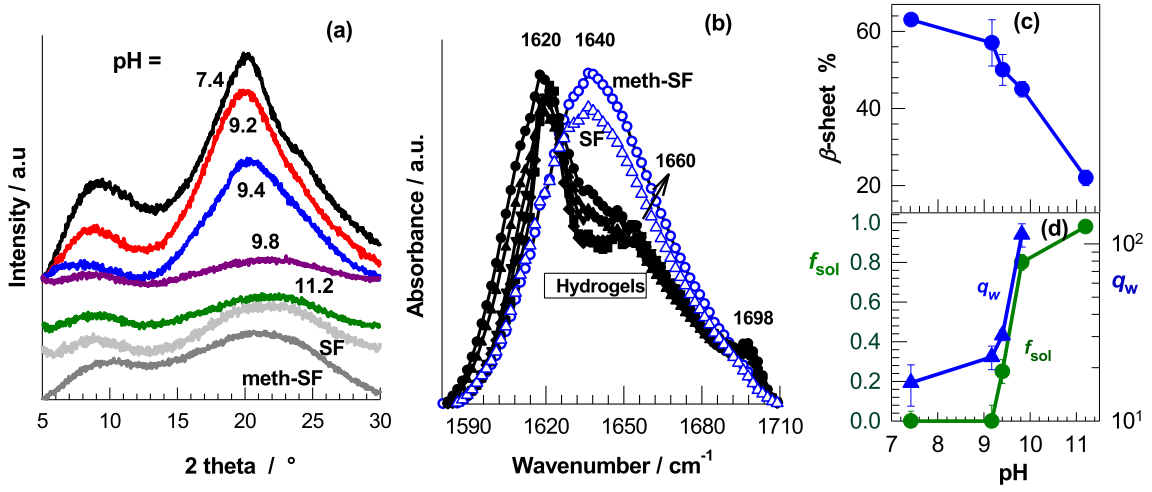

Fig. 3. (a, b): XRD scans (a) and FTIR spectra (b) of the hydrogels prepared at various pHs together with the neat SF and meth-SF. In (b), pH = 7.4 (circle), 9.2 (triangle up), 9.4 (triangle down), 9.8 (diamond), and 11.2 (square). (c, d): β-sheet content (c), soluble fraction f_{sol}, and weight swelling ratio q_w (d) of the hydrogels plotted against the reaction pH.

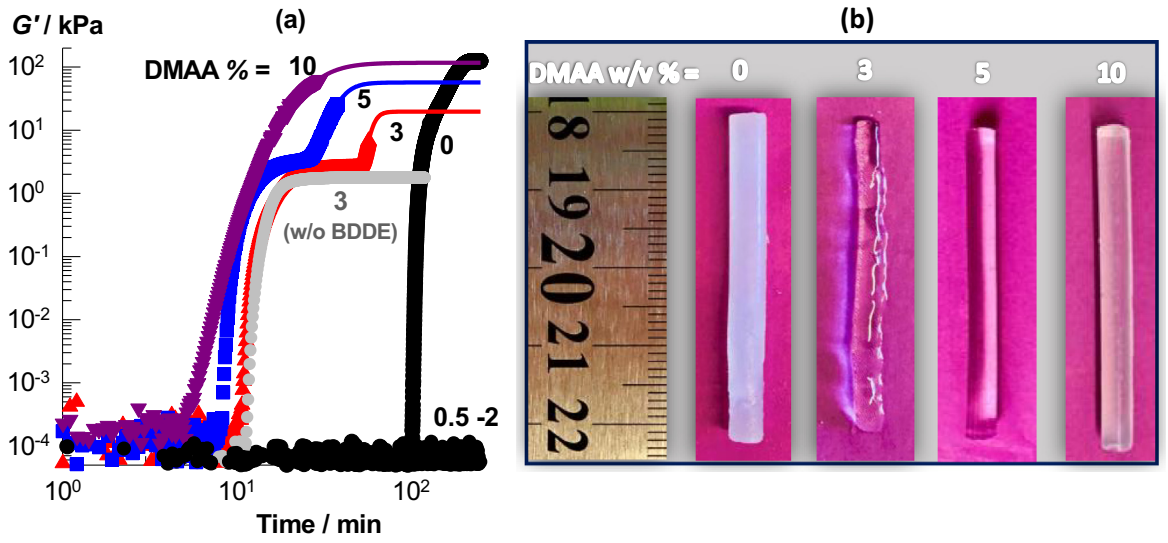

Fig. 4. (a): Reaction time dependence of storage modulus G' of the gelation system at 50 °C and at various DMAA contents as indicated. pH = 7.4. BDDE = 20 mmol·g^{-1}. The gray curve shows the reaction profile with 3% DMAA at 25 °C in the absence of BDDE. $\omega = 6.28$ rad·s^{-1}. $\gamma = 0.01$. (b): Digital images of the hydrogels after a reaction time of 24 h. DMAA concentrations are indicated.

characteristic peaks of PDMAA at 10.5° and 22.8° overlap with those of the β-sheet structure at 9° and 20.1° (Fig. 5b) [17,23,67–69]. However, the broad peak of meth-SF before gelation at around 21° becomes sharper with increasing DMAA content of the hydrogels indicating increasing β-sheet content.

Fig. 6a, b shows frequency dependences of G' and tan δ of the hydrogels at 25 °C prepared at various DMAA contents. As the DMAA content is increased from 2 to 10%, G' continuously increases, and becomes frequency-dependent at high DMAA contents. For instance, at 2% DMAA, G' is 13.3 ± 0.3 kPa over the whole range of frequency, while at 10% DMAA, it is one order of magnitude higher (100–150 kPa), and increases with frequency indicating existence of intermolecular physical bonds acting as effective cross-links at short experimental time scales. Moreover, an abrupt initial decrease in G' is seen after incorporation of 2% DMAA into meth-SF network while further increase in the amount of DMAA again increases G' and approaches to the value of the DMAA-free hydrogel (Figs. 6a, S3). *tan* δ remains below 0.1 up to 7% DMAA which is typical for strong gels with negligible viscous behavior, while it increases above 0.1 at a higher DMAA content indicating formation of a viscoelastic gel. For instance, at ω = 6.28 rad s^{-1}, the hydrogels without and with 10% DMAA have similar modulus G', 110 and 113 kPa, respectively but their loss factors *tan* δ are 0.06 and 0.5, respectively. This reveals that, although the cross-link density of the hydrogel remains unchanged after incorporation of PDMAA chains, these chains significantly contribute to the dissipation of energy under the effect of the oscillatory deformation. The energy dissipation in a gel network is known to improve the ultimate mechanical properties of the hydrogels such as tensile strength and toughness by providing delocalization of the applied force [70]. This is demonstrated in Fig. 6c where the images of two cylindrical hydrogel specimens prepared without and with 10% DMAA are shown. The specimens having the same initial diameters, 4.5 mm, are compressed

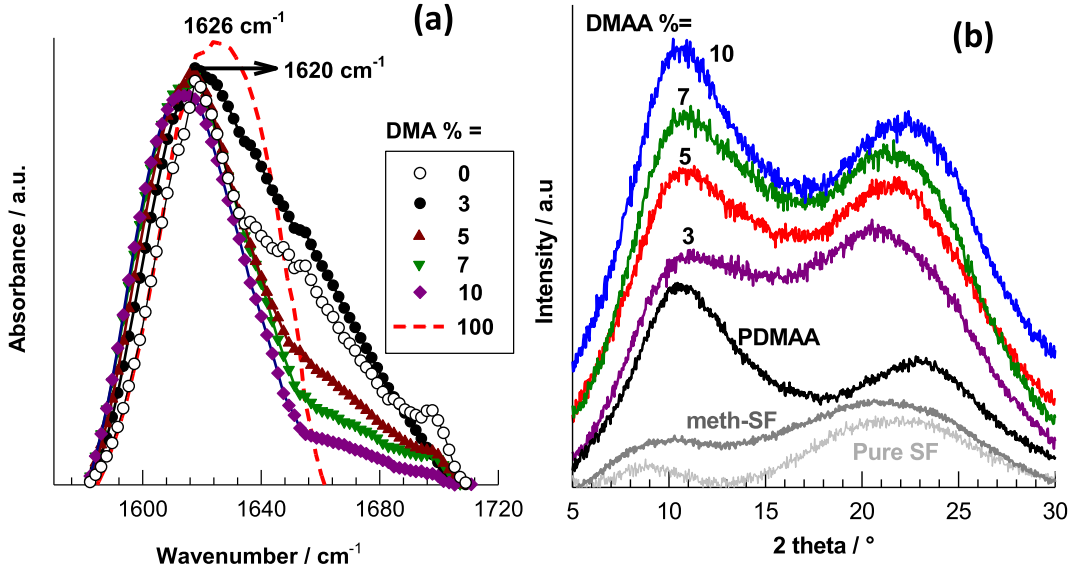

Fig. 5. FTIR spectra (a) and XRD scans (b) of the hydrogels at various DMAA contents, PDMAA, neat SF and meth-SF.

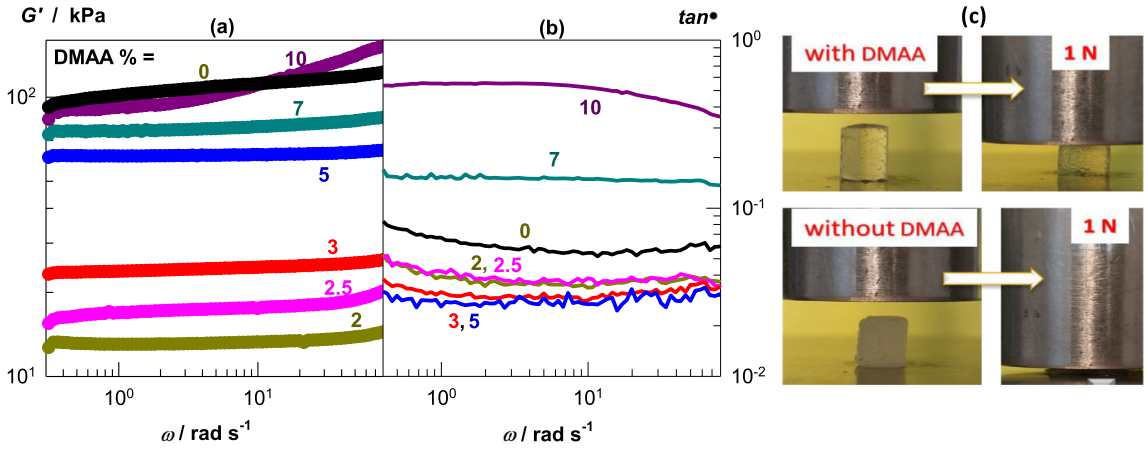

Fig. 6. (a, b): Frequency dependences of G' (a) and $tan\ \delta$ (b) of the hydrogels at 25 °C prepared at various DMAA contents. $\gamma_o = 0.01$. (c): Images showing compression of two cylindrical hydrogel specimens prepared without and with 10% DMAA under a nominal stress of 63 kPa.

under a constant force of 1 N, corresponding to a nominal stress of 63 kPa. Although they both have the same stiffness, the one containing DMAA deforms by 26% without a macroscopic damage, while the other fractures completely. The energy dissipation mechanism in DMAA-containing hydrogel prevents force localization and hence protects the hydrogel network from a macroscopic damage.

Fig. 7a, b shows tensile (a) and compressive stress–strain curves (b) of the hydrogels at various DMAA contents. DMAA-free hydrogel that is brittle in both compression and tension turns into a stretchable and tough one after incorporation of 2–3% DMAA into the meth-SF network (inset to Fig. 7a). For instance, the toughness W of the hydrogel with 2.5% DMAA is 54 ± 4 kJ·m^{-3} during compression which is around 20-fold higher than that of DMAA-free hydrogel (2.5 ± 0.2 kJ·m^{-3}) (Fig. 7c). Moreover, W of the hydrogel with 2.5% DMAA is 10 ± 1 kJ·m^{-3} during tension as compared to the zero-toughness of DMAA-free one. Fig. 7c also shows that W continuously decreases as the DMAA content is further increased up to 10% but still remains at a high level as compared to the DMAA-free hydrogel.

Fig. 8a shows Young's modulus E, and the cross-link density ν_e of the hydrogels plotted against DMAA %. Assuming affine network behavior, the cross-link density ν_e was estimated using the equation [71,72],

$$E = 3\nu_e RT\nu_2^o \quad (2)$$

where R and T have their usual meanings, and ν_2^o is the volume fraction of meth-SF-PDMAA network in as-prepared gel state, calculated by

$$\nu_2^o = c_o(1-f_{sol})/\rho \quad (3)$$

where c_o is the initial DMAA+meth-SF concentration (in g·mL^{-1}) in the reaction solution, and ρ is the polymer density taken as the weight average of the densities of PDMAA and SF (1.21 and 1.35 g·mL^{-1}, respectively [42]). Similar to the storage modulus (Fig. 6a), both Young's modulus E and the cross-link density ν_e decrease by one order of magnitude upon incorporation of 2% DMAA into the hydrogel network while they again increase with a further addition of DMAA. This is in good agreement with the equilibrium weight swelling ratio q_w of the hydrogels in water (Fig. S4); q_w first increases after addition of 2% DMAA but then continuously decreases to approach the q_w of DMAA-free hydrogel. Fig. 8b, c shows fracture strain ε_f and fracture stress σ_f of the hydrogels during elongation (b, left panel) and compression (c, right panel) plotted against DMAA %. The hydrogel with 2% DMAA sustains up to 370 ± 21% elongation and 95 ± 3% compression ratios which are quite high values for SF-based hydrogels. As the DMAA content is further increased, the tensile strength increases while both the compressive strength and elongation ratio at break decrease. The results can be explained with the variation of β-sheet content of the hydrogels depending on their DMAA contents. The brittle-to-ductile transition

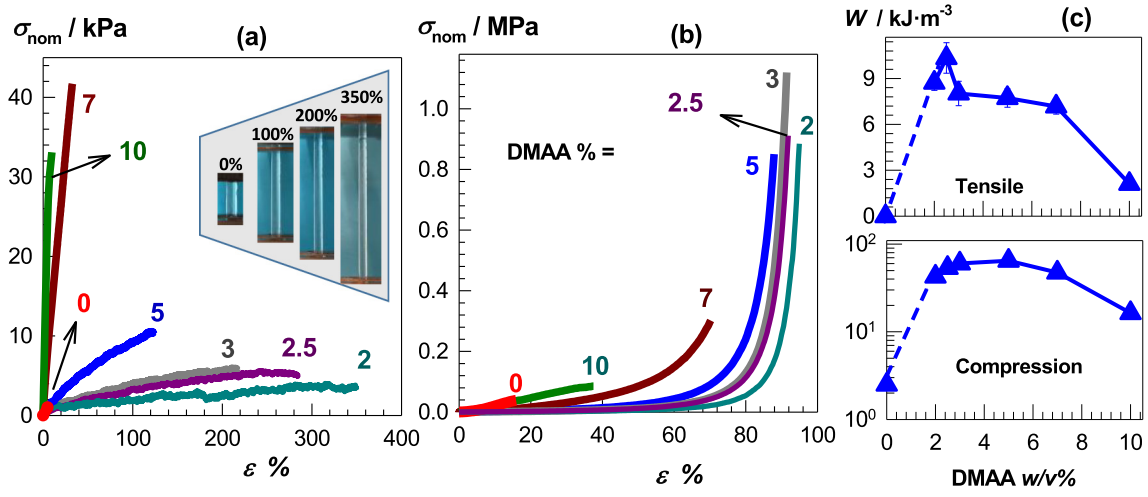

Fig. 7. (a, b): Tensile (a) and compressive stress–strain curves (b) of the hydrogels with various DMAA contents as indicated. The inset shows images of the hydrogel with 2% DMAA during elongation to 350% strain. (c): Energy to break W during tensile (upper panel) and compression tests (bottom panel) plotted against DMAA %.

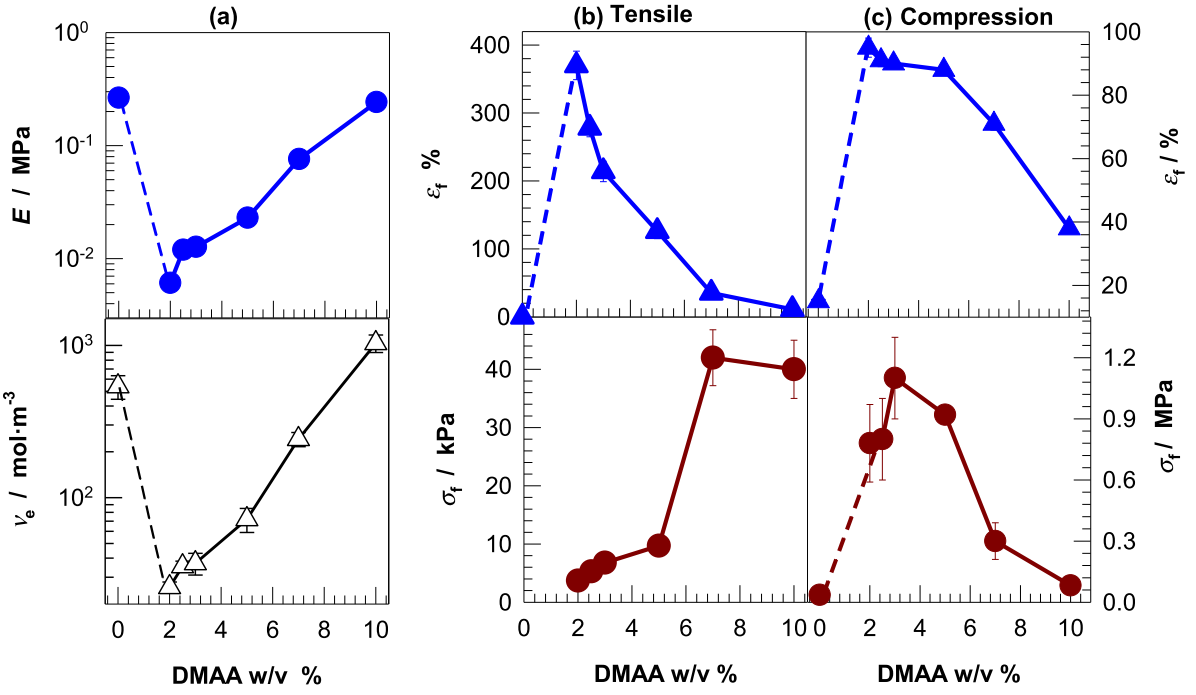

Fig. 8. (a): Young's modulus E and cross-link density ν_e of the hydrogels plotted against DMAA %. (b, c): Mechanical parameters of the hydrogels from uniaxial tensile (b) and compression tests (c) plotted against DMAA %. ε_f = fracture strain, σ_f = fracture stress.

upon incorporation of 2% DMAA could be attributed to the decrease in the β-sheet content of the hydrogels (Figs. 4b, 5). Because the number of β-sheet domains and hence the cross-link density of the hydrogels again increases above 2% DMAA, their stretchability decreases. Moreover, the density of chain-entanglement cross-links between meth-SF and PDMAA also increases with increasing DMAA content leading to better mechanical properties as compared to the DMAA-free hydrogel.

To understand the nature of the cross-links in the hydrogels, cyclic compression tests were conducted to a maximum strain of 30%. Fig. 9a, b shows five successive compression cycles conducted on the hydrogels with 10 and 3% DMAA, denoted as H- and L-hydrogels, respectively. The solid and dashed curves represent loading and unloading curves, respectively. Each unloading curve of H-hydrogel significantly deviates from the previous loading one, indicating the occurrence of an irreversible internal damage in the hydrogel network. In contrast, L-hydrogel exhibits elastic cycles, i.e., each unloading curve closely follows the previous loading with negligible energy dissipation. One may argue that this behavior of L-hydrogel is as a consequence of the lower stress required to compress it by 30% strain as compared to H-hydrogel (7 vs 80 kPa). However, Fig. S5 showing successive compression cycles of L-hydrogel up to 80% strain and 120 kPa stress also reveals its elastic behavior during deformation. This finding indicates deformation of L-hydrogel without formation of any microcracks, which is in accord with its high stretchability as compared to H-hydrogel. Fig. 9c shows the hysteresis energy U_{hys} calculated from the area surrounded by the loading and unloading curves plotted

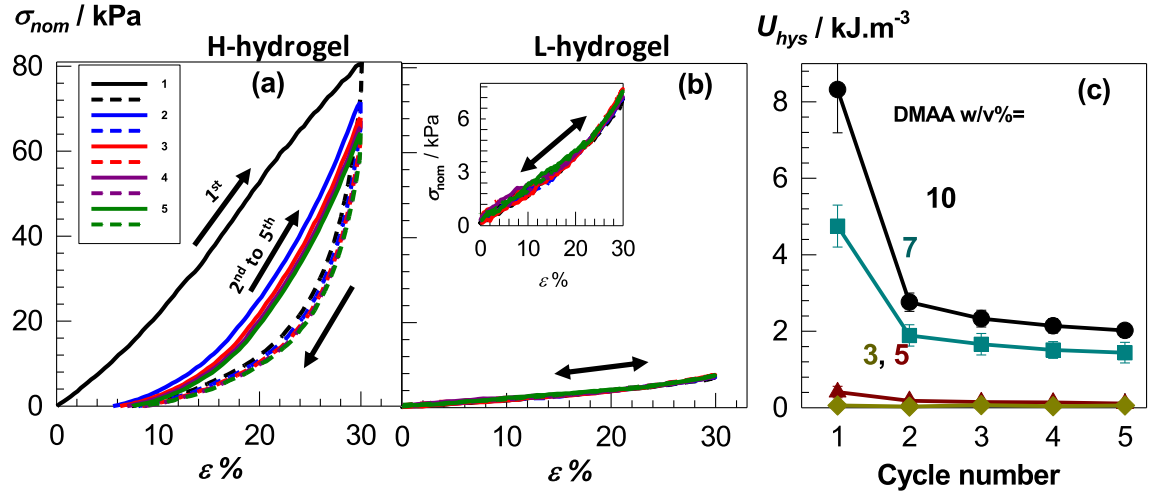

Fig. 9. (a, b): Five successive compression cycles to a maximum strain ε_{max} of 30% conducted on the hydrogels with 10 (a) and 3 w/v % DMAA (b). The solid and dashed curves represent loading and unloading curves, respectively. The inset in (b) is a zoom-in of the data below 7 kPa stress. (c): U_{hys} of the hydrogels with various DMAA contents plotted against the cycle number.

against the number of cycles. As the amount of DMAA is increased from 3 to 10%, U_{hys} of the first cycle increases by two orders of magnitude (from 0.06 to 8.3 kJ·m^{-3}) reflecting increasing extent of internal damage even though the hydrogels remain macroscopically intact. The fraction of dissipated energy f_{diss}, i.e., dissipated energy per loading energy was calculated by dividing U_{hys} to the loading energy (Fig. S6). At 10% DMAA, $f_{diss} = 0.73$, that is, 73% of the loading energy is dissipated whereas f_{diss} decreases to 14% at 3% DMAA.

The experimental findings can be explained according to the following scenario (Scheme 1b): SF molecules are known to exhibit a loose globular structure in aqueous solutions with random coil conformation. When DMAA is added into meth-SF solution, it dissolves in free water as well as in the globular volume formed by meth-SF molecules. Thus, the polymerization of DMAA proceeds both in water and in the globular volume leading to PDMAA chains interconnecting meth-SF globules [47]. Due to the presence of pendant vinyl groups on meth-SF, the globules act as multifunctional cross-linker and lead to the formation of a hydrogel with an interpenetrated and interconnected network structure exhibiting a modulus of around 1 kPa. Because conformational transition in SF requires a longer time than the time required for the polymerization of DMAA [39], formation of β-sheets and hence further increase of the modulus occurs in the second stage of the reaction. Moreover, at low DMAA contents, PDMAA radical chains propagate in a dilute solution which facilitates formation of cyclization reactions within the globules, i.e., the radical chains react with pendant vinyl groups locating on the same SF globule (Scheme 1c). This prevents a macroscopic gel formation as observed at below 2% DMAA concentration. Increasing DMAA contents also increases the number and length of PDMAA chains which facilitate intermolecular cross-linking reactions between the globules as well as β-sheet formation between the globules. As a consequence, the cross-link density of the hydrogels and their β-sheet content increase with increasing amount of DMAA from 2 to 10%. Moreover, physical entanglements between PDMAA and meth-SF molecules create an energy dissipation mechanism whose extent increases with increasing DMAA content of the hydrogels.

4. Conclusions

As the hydrogels based on SF are attractive soft materials in biomedical applications, it is generally a challenge to improve their mechanical properties to extend their service time. We presented a novel strategy for preparing stretchable SF hydrogels by incorporating flexible polymer chains into the brittle SF network, which strengthen the interconnections between the SF globules. We included DMAA monomer and APS initiator into an aqueous SF solution containing BDDE and TEMED to in situ generate flexible PDMAA which is a biocompatible polymer with associative properties. Moreover, instead of SF, meth-SF was used for the gel preparation to create an interconnected SF/PDMAA network. The modulus and hence the cross-link density of SF hydrogels decrease by one order of magnitude upon incorporation of 2% DMAA into the SF network while they again increase with a further addition of DMAA. The hydrogel with 2% DMAA sustains up to 370 ± 21% elongation and 95 ± 3% compression ratios which are quite high values for SF-based hydrogels. As the DMAA content is further increased, the tensile strength increases while both the compressive strength and elongation ratio at break decrease. The results can be explained with the variation of β-sheet content of the hydrogels depending on their DMAA contents. The brittle-to-ductile transition upon incorporation of 2% PDMAA into the SF network could be attributed to the decrease in the β-sheet content of the hydrogels. Moreover, the density of both β-sheet cross-links and chain-entanglements between meth-SF and PDMAA increase with increasing DMAA content leading to better mechanical properties as compared to the DMAA-free hydrogel. The components of meth-SF hydrogels presented here, namely PDMAA [51–53], meth-SF [24], and BDDE-cross-linked biopolymers including SF [73–76] are reported to be biocompatible and non-cytotoxic. Therefore, the stretchable and tough SF hydrogels thus developed are suitable as a scaffold in tissue engineering and offer an advantage as a biomaterial over other SF-based biomaterials.

CRediT authorship contribution statement

Cigdem Buse Oral: Conceptualization; Investigation.
Berkant Yetiskin: Conceptualization; Supervision; Investigation; Writing – review & editing.
Oguz Okay: Conceptualization; Supervision; Writing – review & editing; Funding acquisition; Project administration; Resources;

Acknowledgments

Work was supported by Istanbul Technical University, BAP TDK-2019-42484. O. O. thanks Turkish Academy of Sciences (TUBA) for the partial support.

Appendix A. Supplementary data

Supplementary data to this article can be found online at https://doi.org/10.1016/j.ijbiomac.2020.08.040.

References

[1] C. Vepari, D.L. Kaplan, Silk as a biomaterial, Prog. Polym. Sci. 32 (2007) 991–1007.
[2] J.G. Hardy, L.M. Romer, T.R. Scheibel, Polymeric materials based on silk proteins, Polymer 49 (2008) 4309–4327.
[3] F. Vollrath, D. Porter, Silks as ancient models for modern polymers, Polymer 50 (2009) 5623–5632.
[4] J. Melke, S. Midha, S. Ghosh, K. Ito, S. Hofmann, Silk fibroin as biomaterial for bone tissue engineering, Acta Biomater. 31 (2016) 1–16.
[5] T. Rasheed, M. Bilal, Y. Zhao, A. Raza, S.Z.H. Shah, H.M.N. Iqbal, Physiochemical characteristics and bone/cartilage tissue engineering potentialities of protein-based macromolecules - a review, Int. J. Biol. Macromol. 121 (2019) 13–22.
[6] H.-J. Jin, D.L. Kaplan, Mechanism of silk processing in insects and spiders, Nature 424 (2003) 1057–1061.
[7] C.-Z. Zhou, Fine organization of Bombyx mori fibroin heavy chain gene, Nucleic Acids Res. 28 (2000) 2413–2419.
[8] A.R. Murphy, D.L. Kaplan, Biomedical applications of chemically-modified silk fibroin, J. Mater. Chem. 19 (2009) 6443–6450.
[9] S.V. Vlierberghe, P. Dubruel, E. Schacht, Biopolymer-based hydrogels as scaffolds for tissue engineering applications: a review, Biomacromolecules 12 (2011) 1387–1408.
[10] L.-D. Koh, Y. Chen, C.-P. Teng, Y.-W. Khin, X.-J. Loh, S.-Y. Tee, M. Low, E. Ye, H.-D. Yu, Y.-W. Zhang, M.-Y. Han, Structures, mechanical properties and applications of silk fibroin materials, Prog. Polym. Sci. 46 (2015) 86–110.
[11] R. Zhang, Y. Tao, Q. Xu, N. Liu, P. Chen, Y. Zhou, Z. Bai, Rheological and ion-conductive properties of injectable and self-healing hydrogels based on xanthan gum and silk fibroin, Int. J. Biol. Macromol. 144 (2020) 473–482.
[12] T. Adali, R. Kalkan, L. Karimizarandi, The chondrocyte cell proliferation of a chitosan/silk fibroin/egg shell membrane hydrogels, Int. J. Biol. Macromol. 124 (2019) 541–547.
[13] M.C. Asuncion, J.C. Goh, S.L. Toh, Anisotropic silk fibroin/gelatin scaffolds from unidirectional freezing, Mater. Sci. Eng. C Mater. Biol. Appl. 67 (2016) 646–656.
[14] R. Nazarov, H.-J. Jin, D.L. Kaplan, Porous 3-D scaffolds from regenerated silk fibroin, Biomacromolecules 5 (2014) 718–726.
[15] T. Li, X. Song, C. Weng, X. Wang, L. Gu, X. Gong, Q. Wei, X. Duan, L. Yang, C. Chen, Silk fibroin/carboxymethyl chitosan hydrogel with tunable biomechanical properties has application potential as cartilage scaffold, Int. J. Biol. Macromol. 137 (2019) 382–391.
[16] K. Kaewprasit, T. Kobayashi, S. Damrongsakkul, Thai silk fibroin gelation process enhancing by monohydric and polyhydric alcohols, Int. J. Biol. Macromol. 118 (2018) 1726–1735.
[17] U.J. Kim, J. Park, C. Li, H.J. Jin, R. Valluzzi, D.L. Kaplan, Structure and properties of silk hydrogels, Biomacromolecules 5 (2004) 786–792.
[18] A. Matsumoto, J. Chen, A.L. Collette, U.J. Kim, G.H. Altman, P. Cebe, D.L. Kaplan, Mechanisms of silk fibroin sol-gel transitions, J. Phys. Chem. B 110 (2006) 21630–21638.
[19] C. Dicko, J.M. Kenney, D. Knight, F. Vollrath, Transition to a beta-sheet-rich structure in spidroin in vitro: the effects of pH and cations, Biochemistry 43 (2004) 14080–14087.
[20] T. Yucel, P. Cebe, D.L. Kaplan, Vortex-induced injectable silk fibroin hydrogels, Biophys. J. 97 (2009) 2044–2050.
[21] E. Servoli, D. Maniglio, A. Motta, C. Migliaresi, Folding and assembly of fibroin driven by an AC electric field: effects on film properties, Macromol. Biosci. 8 (2008) 827–835.

[22] I. Karakutuk, F. Ak, O. Okay, Diepoxide-triggered conformational transition of silk fibroin: formation of hydrogels, Biomacromolecules 13 (2012) 1122–1128.
[23] F. Ak, Z. Oztoprak, I. Karakutuk, O. Okay, Macroporous silk fibroin cryogels, Biomacromolecules 14 (2013) 719–727.
[24] S.H. Kim, Y.K. Yeon, J.M. Lee, J.R. Chao, Y.J. Lee, Y.B. Seo, M.T. Sultan, O.J. Lee, J.S. Lee, S.-il Yoon, I.-S. Hong, G. Khang, S.J. Lee, J.J. Yoo, C.H. Park, Precisely printable and biocompatible silk fibroin bioink for digital light processing 3D printing, Nat. Commun. 9 (2018) 1620.
[25] B.P. Partlow, C.W. Hanna, J. Rnjak-Kovacina, J.E. Moreau, M.B. Applegate, K.A. Burke, B. Marelli, A.N. Mitropoulos, F.G. Omenetto, D.L. Kaplan, Highly tunable elastomeric silk biomaterials, Adv. Funct. Mater. 24 (2014) 4615–4624.
[26] D. Kuang, F. Jiang, F. Wu, K. Kaur, S. Ghosh, S.C. Kundu, S. Lu, Highly elastomeric photocurable silk hydrogels, Int. J. Biol. Macromol. 134 (2019) 838–845.
[27] Y. Zhou, K. Liang, S. Zhao, C. Zhang, J. Li, H. Yang, X. Liu, X. Yin, D. Chen, W. Xu, P. Xiao, Photopolymerized maleilated chitosan/methacrylated silk fibroin micro/nanocomposite hydrogels as potential scaffolds for cartilage tissue engineering, Int. J. Biol. Macromol. 108 (2018) 383–390.
[28] D. Su, M. Yao, J. Liu, Y. Zhong, X. Chen, Z. Shao, Enhancing mechanical properties of silk fibroin hydrogel through restricting the growth of β-sheet domains, ACS Appl. Mater. Interfaces 9 (2017) 17489–17498.
[29] Z. Li, Z. Zheng, Y. Yang, G. Fang, J. Yao, Z. Shao, X. Chen, Robust protein hydrogels from silkworm silk, ACS Sustain. Chem. Eng. 4 (2016) 1500–1506.
[30] F. Chen, S. Lu, L. Zhu, Z. Tang, Q. Wang, G. Qin, J. Yang, G. Sun, Q. Zhang, Q. Chen, Conductive regenerated silk-fibroin-based hydrogels with integrated high mechanical performances, J. Mater. Chem. B 7 (2019) 1708–1715.
[31] M. Yao, D. Su, W. Wang, X. Chen, Z. Shao, Fabrication of air-stable and conductive silk fibroin gels, ACS Appl. Mater. Interfaces 10 (2018) 38466–38475.
[32] Y. Zhao, J. Guan, S.J. Wu, Highly stretchable and tough physical silk fibroin–based double network hydrogels, Macromol. Rapid Commun. 40 (1–5) (2019) 1900389.
[33] D. Kuang, F. Wu, Z. Yin, T. Zhu, T. Xing, S.C. Kundu, S. Lu, Silk fibroin/polyvinyl pyrrolidone interpenetrating polymer network hydrogels, Polymers 10 (2018) 1–11 153.
[34] B.B. Mandal, S. Kapoor, S.C. Kundu, Silk fibroin/polyacrylamide semi-interpenetrating network hydrogels for controlled drug release, Biomaterials 30 (2009) 2826–2836.
[35] F.G. Roca, P.L. Picazo, J. Perez-Rigueiro, G.V.G. Tortuero, M.M. Pradas, C. Martinez-Ramos, Conduits based on the combination of hyaluronic acid and silk fibroin: characterization, in vitro studies and in vivo biocompatibility, Int. J. Biol. Macromol. 48 (2020) 378–390.
[36] M. Abbasian, B. Massoumi, R. Mohammad-Rezaei, H. Samadian, M. Jaymand, Scaffolding polymeric biomaterials: are naturally occurring biological macromolecules more appropriate for tissue engineering? Int. J. Biol. Macromol. 134 (2019) 673–694.
[37] T. Li, X. Song, C. Weng, X. Wang, J. Wu, L. Sun, X. Gong, W.-N. Zeng, L. Yang, C. Chen, Enzymatically crosslinked and mechanically tunable silk fibroin/pullulan hydrogels for mesenchymal stem cells delivery, Int. J. Biol. Macromol. 115 (2018) 300–307.
[38] W. Xiao, J. He, J.W. Nichol, L. Wang, C.B. Hutson, B. Wang, Y. Du, H. Fan, A. Khademhosseini, Synthesis and characterization of photocrosslinkable gelatin and silk fibroin interpenetrating polymer network hydrogels, Acta Biomater. 7 (2011) 2384–2393.
[39] B. Tavsanli, O. Okay, Mechanically robust and stretchable silk/hyaluronic acid hydrogels, Carbohydr. Polym. 208 (2019) 413–420.
[40] S. Yan, Q. Wang, Z. Tariq, R. You, X. Li, M. Li, Q. Zhang, Facile preparation of bioactive silk fibroin/hyaluronic acid hydrogels, Int. J. Biol. Macromol. 118 (2018) 775–782.
[41] B. Yetiskin, O. Okay, High-strength and self-recoverable silk fibroin cryogels with anisotropic swelling and mechanical properties, Int. J. Biol. Macromol. 122 (2019) 1279–1289.
[42] B. Yetiskin, C. Akinci, O. Okay, Cryogelation within cryogels: silk fibroin scaffolds with single-, double- and triple-network structures, Polymer 128 (2017) 47–56.
[43] B. Yetiskin, O. Okay, High-strength silk fibroin scaffolds with anisotropic mechanical properties, Polymer 112 (2017) 61–70.
[44] W. Yang, H. Xu, Y. Lan, Q. Zhu, Y. Liu, S. Huang, S. Shi, A. Hancharou, B. Tang, R. Guo, Preparation and characterisation of a novel silk fibroin/hyaluronic acid/sodium alginate scaffold for skin repair, Int. J. Biol. Macromol. 130 (2019) 58–67.
[45] X. Li, S. Yan, J. Qu, M. Li, D. Ye, R. You, Q. Zhang, D. Wang, Soft freezing-induced self-assembly of silk fibroin for tunable gelation, Int. J. Biol. Macromol. 117 (2018) 691–695.
[46] Q. Lu, H. Zhu, C. Zhang, F. Zhang, B. Zhang, D.L. Kaplan, Silk self-assembly mechanisms and control-from thermodynamics to kinetics, Biomacromolecules 13 (2012) 826–832.
[47] J.L. Whittaker, R. Balu, R. Knott, L. de Campo, J.P. Mata, C. Rehm, A.J. Hill, N.K. Dutta, N.R. Choudhury, Structural evolution of photocrosslinked silk fibroin and silk fibroin-based hybrid hydrogels: a small angle and ultra-small angle scattering investigation, Int. J. Biol. Macromol. 114 (2018) 998–1007.
[48] M.M. Ozmen, O. Okay, Non-Gaussian elasticity of poly(2-acrylamido-2-methylpropane sulfonic acid) gels, Polym. Bull. 52 (2004) 83–90.
[49] Y. Uemura, J. McNulty, P.M. Macdonald, Associative behavior and diffusion coefficients of hydrophobically modified poly(N,N-dimethylacrylamides), Macromolecules 28 (1995) 4150–4158.
[50] A.T. Uzumcu, O. Guney, O. Okay, Highly stretchable DNA/clay hydrogels with self-healing ability, ACS Appl. Mater. Interfaces 10 (2018) 8296–8306.
[51] A.A.A. de Queiroz, S.C. Castro, O.Z. Higa, Adsorption of plasma proteins to DMAA hydrogels obtained by ionizing radiation and its relationship with blood compatibility, J. Biomater. Sci. Polym. Edn. 8 (1997) 335–347.
[52] M. Babic, D. Horak, P. Jendelova, K. Glogarova, V. Herynek, M. Trchova, K. Likavcanova, P. Lesny, E. Pollert, M. Hajek, E. Sykova, Poly(N,N-dimethylacrylamide)-coated maghemite nanoparticles for stem cell labeling, Bioconjug. Chem. 20 (2009) 283–294.
[53] L. Weng, A. Gouldstone, Y. Wu, W. Chen, Mechanically strong double network photocrosslinked hydrogels from N,N-dimethylacrylamide and glycidyl methacrylated hyaluronan, Biomaterials 29 (2008) 2153–2163.
[54] X. Chen, D.P. Knight, Z. Shao, F. Vollrath, Conformation transition in silk protein films monitored by time-resolved Fourier transform infrared spectroscopy: effect of potassium ions on Nephila spidroin films, Biochemistry 41 (2002) 14944–14950.
[55] C. Mo, C. Holland, D. Porter, Z. Shao, F. Vollrath, Concentration state dependence of the rheological and structural properties of reconstituted silk, Biomacromolecules 10 (2009) 2724–2728.
[56] H.-J. Jin, J. Park, V. Karageorgiou, U.-J. Kim, R. Valluzzi, P. Cebe, D.L. Kaplan, Water-stable silk films with reduced β-sheet content, Adv. Funct. Mater. 15 (2005) 1241–1247.
[57] Q. Lu, X. Hu, X. Wang, J.A. Kluge, S. Lu, P. Cebe, D.L. Kaplan, Water-insoluble silk films with silk I structure, Acta Biomater. 6 (2010) 1380–1387.
[58] J. Hua, H. You, X. Li, R. You, L. Ma, Cu(II) ion loading in silk fibroin scaffolds with silk I structure, Int. J. Biol. Macromol. 58 (2020) 275–281.
[59] P. Cebe, B.P. Partlow, D.L. Kaplan, A. Wurm, E. Zhuravlev, C. Schick, Silk I and silk II studied by fast scanning calorimetry, Acta Biomater. 55 (2017) 323–332.
[60] J. Giraldo, N.M. Vivas, E. Vila, A. Badia, Assessing the (a)symmetry of concentration-effect curves: empirical versus mechanistic models, Pharmacol. Therapeut. 95 (2002) 21–45.
[61] D. Calvet, J.Y. Wong, S. Giasson, Rheological monitoring of polyacrylamide gelation: importance of cross-link density and temperature, Macromolecules 37 (2004) 7762–7771.
[62] O. Okay, W. Oppermann, Polyacrylamide - clay nanocomposite hydrogels: rheological and light scattering characterization, Macromolecules 40 (2007) 3378–3387.
[63] A. Argun, V. Can, U. Altun, O. Okay, Nonionic double and triple network hydrogels of high mechanical strength, Macromolecules 47 (2014) 6430–6440.
[64] R. Zeeman, P.J. Dijkstra, P.B. van Wachem, M.J.A. van Luyn, M. Hendriks, P.T. Cahalan, J. Feijen, The kinetics of 1,4-butanediol diglycidyl ether crosslinking of dermal sheep collagen, J. Biomed. Mater. Res. 51 (2000) 541–548.
[65] S.B. Ross-Murphy, V.J. Morris, E.R. Morris, Molecular viscoelasticity of xanthan polysaccharide, Faraday Symp. Chem. Soc. 18 (1983) 115–129.
[66] S.B. Ross-Murphy, Structure–property relationships in food biopolymer gels and solutions, J. Rheol. 39 (1995) 1451–1463.
[67] Z.H. Ayub, M. Arai, K. Hirabayashi, Mechanism of the gelation of fibroin solution, Biosci. Biotechnol. Biochem. 57 (1993) 1910–1912.
[68] K. Haraguchi, R. Farnworth, A. Ohbayashi, T. Takehisa, Compositional effects on mechanical properties of nanocomposite hydrogels composed of poly(N,N-dimethylacrylamide) and clay, Macromolecules 36 (2003) 5732–5741.
[69] R. Naohara, K. Narita, T. Ikeda-Fukazawa, Change in hydrogen bonding structures of a hydrogel with dehydration, Chem. Phys. Lett. 670 (2017) 84–88.
[70] H.R. Brown, A model of the fracture of double network gels, Macromolecules 40 (2007) 3815–3818.
[71] P.J. Flory, Principles of Polymer Chemistry, Cornell University Press, Ithaca, NY, 1953.
[72] L.R.G. Treloar, The Physics of Rubber Elasticity, 3rd ed. Oxford University Press, USA, 1975.
[73] T.-W. Chung, W.-P. Chen, P.-W. Tai, H.-Y. Lo, T.-Y. Wu, Roles of silk fibroin on characteristics of hyaluronic acid/silk fibroin hydrogels for tissue engineering of nucleus pulposus, Materials 13 (1–18) (2020) 2750.
[74] S.-M. Lan, I.-.M. Jou, P.-T. Wu, C.-Y. Wu, S.-C. Chen, Investigation into the safety of perineural application of 1,4-butanediol diglycidyl ether-crosslinked hyaluronan in a rat model, J. Biomed. Mater. Res. Part B 103B (2015) 718–726.
[75] L.B. Koh, M.M. Islam, D. Mitra, C.W. Noel, K. Merrett, S. Odorcic, P. Fagerholm, W.B. Jackson, B. Liedberg, J. Phopase, M. Griffith, Epoxy cross-linked collagen and collagen-laminin peptide hydrogels as corneal substitutes, J. Funct. Biomater. 4 (2013) 162–177.
[76] J.R. Dias, S. Baptista-Silva, C.M.T. de Oliveira, A. Sousa, A.L. Oliveira, P.J. Bártolo, P.L. Granja, In situ crosslinked electrospun gelatin nanofibers for skin regeneration, Eur. Polym. J. 95 (2017) 161–173.